

# Light-Directed Writing of Chemically Tunable Narrow-Band Holographic Sensors

Ali K. Yetisen,\* Haider Butt, Fernando da Cruz Vasconcellos, Yunuen Montelongo, Colin A. B. Davidson, Jeff Blyth, Leon Chan, J. Bryan Carmody, Silvia Vignolini, Ullrich Steiner, Jeremy J. Baumberg, Timothy D. Wilkinson, and Christopher R. Lowe

Dynamic photonic structures can be tuned by changing the periodic structure and/or the index of refraction.<sup>[1]</sup> These dynamic photonic structures allow optically responsive capability to control the properties of light and act as optical transducers to sense external stimuli.<sup>[2]</sup> Tunable optical systems operating in the visible and near-infrared region offer great promise for designing adaptive optical materials, telecommunication devices and sensors. Such sensors have been prepared by various methods, including microfabrication, self-assembly or a combination of both.<sup>[3]</sup> However, achieving the attributes of a narrow-band response with a high-tunability range to construct off-axis optical sensors still remains a significant challenge.

We recently developed an optical sensing platform<sup>[4]</sup> based on Denisjuk reflection holography<sup>[5]</sup> and in situ size reduction of metallic nanoparticles in polymers through laser ablation, where an intense laser pulse produces Bragg gratings in a fraction of the time, cost and complexity compared to silver-halide chemistry-based fabrication techniques.<sup>[6]</sup> This technique allows the fabrication of holographic sensors that display improved versatility and scalability. The platform utilizes an efficient approach to produce off-axis chemical-stimuli responsive holographic sensors with a large, reversible narrow-band tunability, using metallic nanoparticles that can be organized in density-concentrated 3D regions.

The present work employs a hologram fabricated by laser ablation comprising of a functionalized hydrophilic host

polymer. The optical characteristics of the system were investigated by analyzing the distribution of the mean diameter of Ag<sup>0</sup> nanoparticles, effective refractive indices of ablated and non-ablated polymer-nanoparticle regions, along with angular-resolved measurements. Furthermore, the system was characterized through computational modeling and diffraction simulations. The putative clinical utility of the sensor for the quantification of pH was demonstrated with large wavelength shifts in the entire visible spectrum.

Our sensor employs a simultaneous lateral and vertical periodic diffraction grating of silver nanoparticles dispersed within a poly (hydroxyethyl methacrylate)-based (pHEMA) matrix with a dry thickness of approximately 10  $\mu\text{m}$ . The diffracted light is spectrally concentrated at a specific narrowband color due to the vertically-ordered periodicity. We use 6 ns-pulsed laser ( $\lambda = 532 \text{ nm}$ , 240 mJ) standing waves to order the density of silver nanoparticles (mean diameter of  $13 \pm 9 \text{ nm}$ ) into regions with a periodicity of approximately half of the wavelength distributed throughout the cross section of the polymer matrix (see Supporting Information). The fabrication of the holographic sensors begins with UV-initiated free radical polymerization of the pHEMA-based hydrogel on an O<sub>2</sub>-plasma-treated poly (methyl methacrylate) (PMMA) substrate (Figure 1(a)). Subsequently, Ag<sup>+</sup> ions are perfused into the pHEMA polymer matrix (Figure 1(b)), and reduced with a photographic developer to form silver nanoparticles (Ag<sup>0</sup>) (Figure 1(c)). The Ag NPs within the hydrogel matrix are selectively and photochemically patterned at the areas where laser light constructively interferes to form a well-ordered photonic structure (Figure 1(d)) (see Supporting Information). The resulting hologram is instantaneously useable and it acts as a sensor by undergoing changes in diffraction properties during swelling and shrinking in the presence of analytes (Figure 1(e,f)). Our holographic sensor can be functionalized with, for example, methacrylic acid (MAA) that reversibly binds H<sup>+</sup>, and is therefore sensitive to changes in pH. The deprotonation, and hence ionization, of carboxyl groups in MAA, increases the osmotic pressure within the hydrogel. Consequently, this results in water uptake, swells the hydrogel and increases the spacing of the nanoparticles, primarily in the vertical (and to a much lesser extent in the lateral) direction, which produces a dynamic narrow-band diffraction regime. As the concentration of H<sup>+</sup> decreases from pH 4.00 to pH 8.00 under physiological (150 mM) ionic strengths, the wavelength of the peak originating from the structure systematically shifts from 495 to 815 nm (Figure 2(a)). The shift in the diffraction peak is visible to the naked eye throughout most of the measurement

A. K. Yetisen, Dr. F. da Cruz. Vasconcellos,  
Dr. C. A. B. Davidson, Dr. J. Blyth, L. Chan,  
Prof. C. R. Lowe  
Department of Chemical Engineering and Biotechnology  
University of Cambridge  
Tennis Court Road, Cambridge, CB21QT, UK  
E-mail: ay283@cam.ac.uk

Dr. H. Butt, Dr. Y. Montelongo, Prof. T. D. Wilkinson  
Electrical Engineering Division  
Department of Engineering  
University of Cambridge  
Cambridge, CB3 0FA, UK

Dr. S. Vignolini, Prof. U. Steiner, Prof. J. J. Baumberg  
Cavendish Laboratory  
Department of Physics  
University of Cambridge  
J. J. Thomson Avenue, Cambridge, CB3 0HE, UK

Dr. J. B. Carmody  
The Children's Hospital of the King's Daughters  
Norfolk, 23507, VA, USA



DOI: 10.1002/adom.201300375

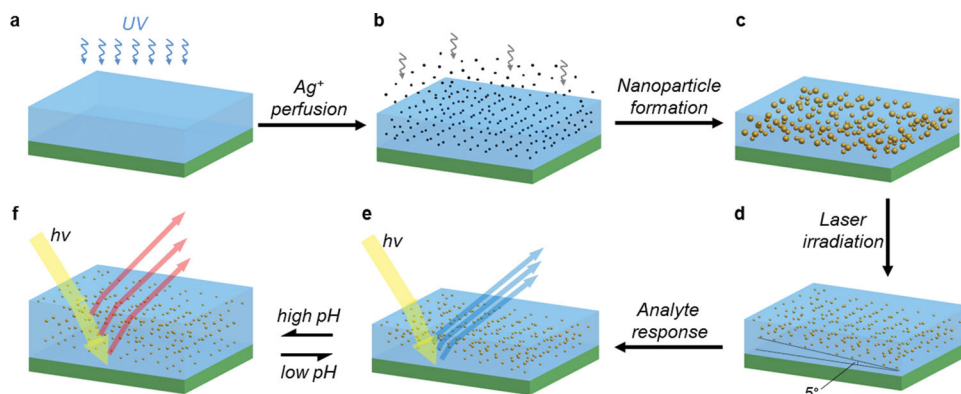


**Figure 1.** Fabrication and tuning of holographic sensors. (a) HEMA monomers functionalized with carboxyl groups were polymerized on an O<sub>2</sub>-plasma-treated PMMA substrate. (b) Ag<sup>+</sup> ions were perfused into pHEMA hydrogel film. (c) Ag<sup>+</sup> ions were reduced to metallic Ag<sup>0</sup> nanoparticles in the pHEMA hydrogel film using a photographic developer. (d) A holographic sensor was formed by photochemically patterning pHEMA-Ag nanoparticle system via a single 6 ns Nd:YAG pulsed laser beam, elevated at 5° from the normal and backed by a mirror. (e) Swelling/shrinking of the holographic sensor by a reagent modulates both the domain spacing and the refractive-index contrast, and systematically shifts the diffracted wavelengths of light ( $h\nu$ ) from 500 to (f) 815 nm when the hydrogel expands in the direction normal to underlying substrate.

cycle (Figure 2(b)). As the hologram expands, the diffraction efficiency decreases (the intensity of the peaks). This trend can be attributed to the decrease in the density of nanoparticles pre-

sent in the periodic regions of the hologram, which reduces the effective index contrast between these regions and the medium (see Supporting Information). Another contributing factor is

that the scattering strength of each Ag<sup>0</sup> NP increases at Mie plasmon resonances in the blue/green region, so the total amount of scattering decreases as the Bragg resonance shifts to longer wavelengths. The entire sensing process is reversible and the same sensor may be used for multiple analyses.

In addition to holographic sensing technology, several advances in pH sensing have been recently demonstrated. New electrochemical and field-effect transistor based sensors have utilized carbon fiber<sup>[7]</sup> and carbon/metallic<sup>[8]</sup> nanostructures for pH sensing, respectively. Notably, recent fluorescent sensors based on Förster resonance energy transfer using synthetic DNA,<sup>[9]</sup> genetically encoded red protein<sup>[10]</sup> and an antibody-conjugated pH dependent dye<sup>[11]</sup> have been demonstrated for intracellular monitoring. Our holographic pH sensor offers unique attributes since it provides not only the interrogation and reporting transducer, but it also has the analyte-responsive hydrogel, rendering it label-free and reusable with remote sensing capability. Our flash photochemical process represents a first step towards multifunctional 3D hydrogel-based holographic sensors.

The response of the holographic sensor to pH change is rapid and reproducible. Consecutive swelling/shrinking steps were reproducible to within  $\pm 3$  nm over 20 successive buffer changes. No hysteresis was detected. For example, a pH change of 0.50 units from pH 5.50 to 6.00 took  $50 \pm 10$  s to equilibrate, with a variation of peak diffraction

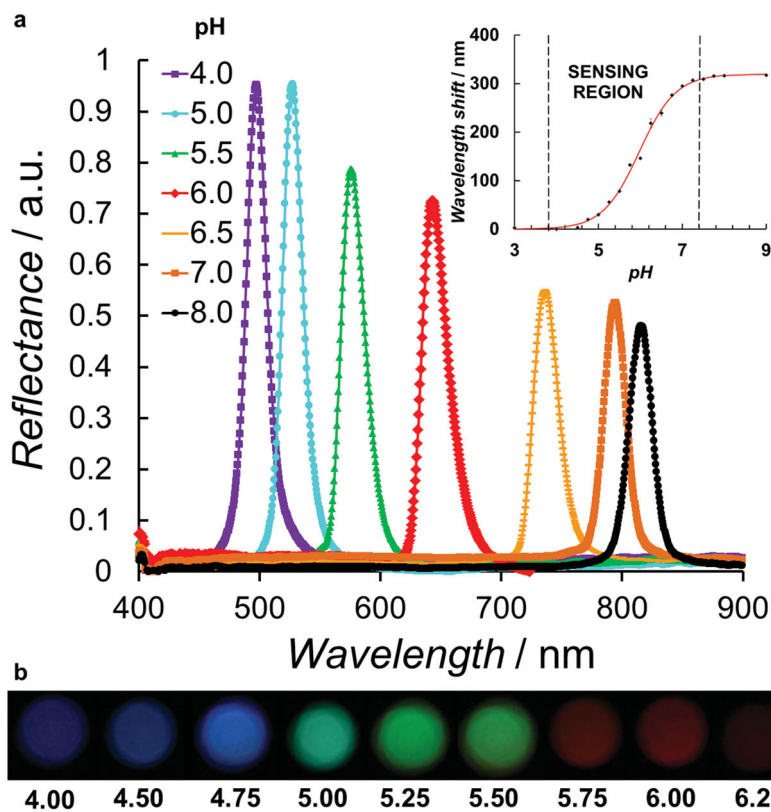


**Figure 2.** Tuning a holographic sensor by variation of pH. (a) Visible-near-infrared diffraction spectra of a holographic sensor swollen by different pH values using phosphate buffers. The largest wavelength shift is at 815 nm and the smallest is at 495 nm, a change of 165%. The inset illustrates the sensor response over three trials. The apparent pK<sub>a</sub> value was calculated as 5.98 using the Henderson-Hasselbalch equation (see Supporting Information). (b) Photographs of the pH-responsive holographic film immersed in phosphate buffers of pH 4.00–6.25. The images were taken under white light illumination.

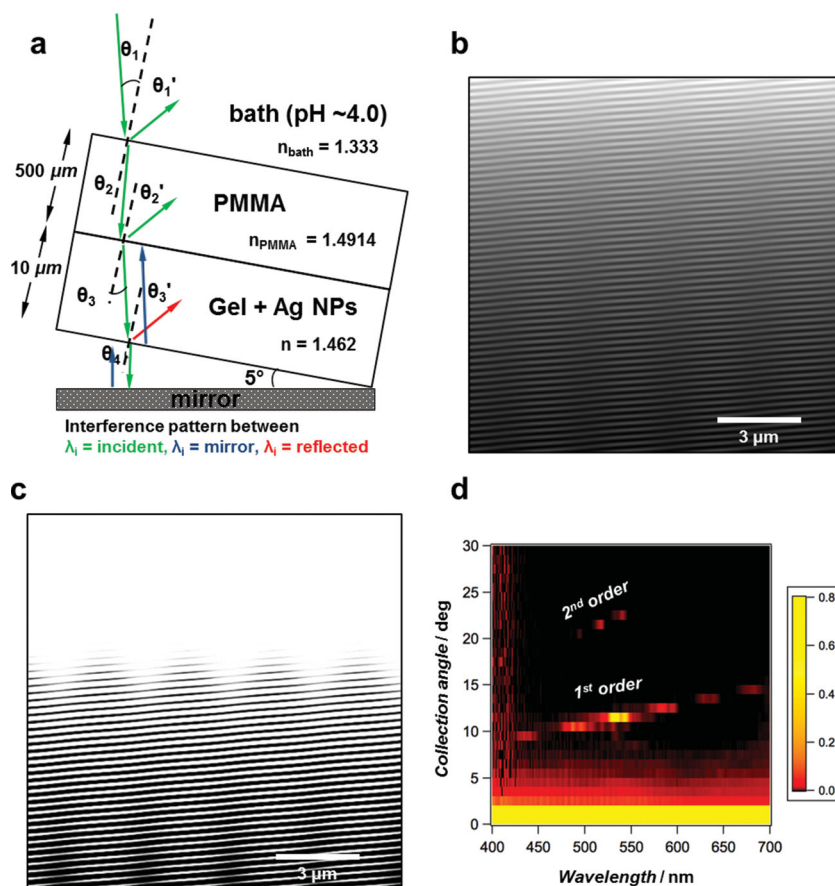


**Figure 3.** Photochemical patterning process based on the interference of multiple beams forms a well-ordered intensity field distribution. (a) Schematic of the laser-based photochemical patterning setup for the preparation of holograms, (b) Schematic of laser light interference beams inside the hydrogel, created from three beams: (1) incident beam, (2) beam reflected from mirror and (3) beam reflected internally at the hydrogel-water interface, (c) Intensity field distribution obtained from a holographic sensor with a tilting angle of  $5^\circ$ . (d) Angular resolved measurements from the photonic structure. The zero order of diffraction ( $0^\circ$ ) is saturated to highlight the presence of the first and second diffracted orders. The intensity is in logarithmic scale. Using the grating equation and measuring the position of the order from the data, we estimate that the grating has a spacing of  $3.01 \mu\text{m}$ .

wavelength of  $\pm 1 \text{ nm}$  over three trials. The pH-sensing range and the sensitivity of the sensor can be controlled through variation of the nature of the ionizable co-monomer in the polymer matrix and its concentration, respectively. For instance, to achieve sensitivity at acidic and alkaline pH, the polymer matrix can be functionalized with MAA and 2-(dimethylamino)ethyl methacrylate ( $\text{p}K_a = 8.40$ ).<sup>[6d]</sup> In order to extend the range, a mixture of ionizable monomers can be co-polymerized. Such hydrogels can also be functionalized to be highly selective to a range of stimuli.<sup>[12]</sup>

In order to predict the interference patterns which produce the photonic structure in the hydrogel, we modeled our system during fabrication as arising from a superposition of different light waves. Hence, we evaluated the interference pattern created from three waves: (1) the incident beam, (2) the beam reflected from the mirror and (3) the beam reflected internally at the hydrogel-water interface. **Figure 3(a)** illustrates a schematic of the laser light interference from the three beams.

The wave vectors ( $K$ ) of these beams can be calculated as previously shown.<sup>[13]</sup>

We reconstructed the intensity distribution of the field along the hydrogel by simulating the interference of the three plane waves. Through computing the respective intensities and phases of individual plane waves, the resulting interference pattern was extracted. To visualize the intensity distribution in a 2D cross-section plane, the electromagnetic field in every point over an area of  $10 \times 10 \mu\text{m}^2$  inside the hydrogel was evaluated. **Figure 3(b)** shows the result for the interference pattern of the three distinct plane waves, taking into account: the angle, index of refraction, laser light wavelength, exponential decay of laser intensity while the laser light travels through the hydrogel-NP system and the laser light phase changes upon reflection.

In order to simulate the laser-based photochemical patterning process, it is assumed that the energy of a single pulse gets transmitted instantaneously (6 ns, 240 mJ) to the particles before heat diffusion is involved. Notably, the localization of heat along the standing wave is essential to produce a well-defined photonic structure. The model was simplified by implying that photochemical patterning process occurs where the energy concentration exceeds a given threshold. **Figure 3(c)** shows the simulation of the resulting structure after photochemical patterning. White regions represent photochemically patterned material while black regions show non-patterned material. Along with the vertical standing wave ( $\sim 193 \text{ nm}$ ), a larger period wave ( $\sim 3 \mu\text{m}$ ) appears in the horizontal direction. The addition of the two standing waves results in a grating-like structure at the interface of the non-patterned region. The effect of laser wavelength, power, pulse duration,

nanoparticle size and surface plasmon resonance on the mechanism of laser-based photochemical patterning and subsequent absorption by the nanoparticles has been discussed elsewhere.<sup>[14]</sup> Studies have shown that the interaction between the laser light and the nanoparticles in situ may influence particle diffusion, oxidation, structure and distribution.<sup>[15]</sup> The outlined factors above could contribute to organizing the nanoparticle-polymer system which acts as a holographic sensor.

In order to characterize the spectral response of the underlying photonic structure, the holographic sensor was illuminated at normal incidence with a supercontinuum white light laser. The backscatter was recorded at different angles by a spectrophotometer positioned onto a goniometer. **Figure 3(d)** illustrates the spectra recorded for different collection angles and the intensity of the peak (in red-to-yellow color scale). The grating structure diffracts light analogous to a blazed (saw tooth) grating. However, the diffraction is two orders of magnitude more efficient at  $\sim 532 \text{ nm}$  compared with the other diffracted

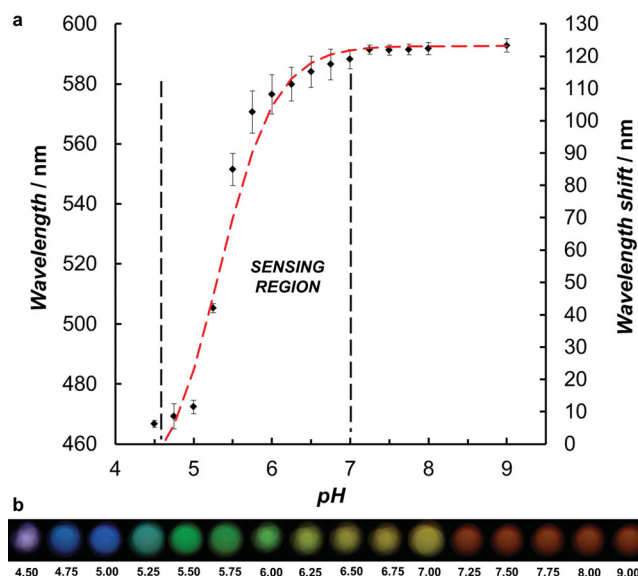


**Figure 4.** (a) Wavelength shift of a holographic sensor swollen by contact with different pH of artificial urine samples over the physiological range. Standard error bars represent three independent samples. The apparent pKa value was calculated as 5.20 using the Henderson-Hasselbalch equation. (b) Photographs of the pH-responsive holographic film sensor response to artificial urine samples (pH 4.5–9.0). The images were taken under white light illumination.

wavelengths (Figure 2(a)), due to the underlying grating multi-layer structure parallel to the grazing surface. The combination of these two structures effectively provides an intense color-selective backscatter at angles away from the sample normal (see Supporting Information).

To demonstrate the utility of our sensor, we describe a clinical application to analyze acid-base balance in artificial urine samples<sup>[16]</sup> (see Supporting Information). Urine pH in a healthy individual is in the range of 5.0–9.0.<sup>[17]</sup> Analysis of urine pH has diagnostic utility in, for example, the evaluation of urinary tract infections (UTIs)<sup>[18]</sup> and renal tubular acidosis.<sup>[19]</sup> Modification of the urine pH is a key element of treatment for certain types of kidney stones,<sup>[20]</sup> or toxic ingestions.<sup>[21]</sup> We have tailored the tunability range of our holographic sensors to measure the pH from 4.5–7.0 in artificial urine samples. **Figure 4(a)** shows the holographic sensor's wavelength shift as a function of pH in the physiological range. The sensor has exceptional sensitivity from pH 4.6–6.6. This wavelength range can be tuned anywhere from UV to near infrared. **Figure 4(b)** presents the corresponding colorimetric response. The spectrophotometer had a resolution of 0.5 nm wavelength shift, which corresponds to a minimum lattice swelling distance of 0.18 nm, obeying the Bragg's law ( $\lambda_{\text{peak}} = 2 n d \cos(\theta)$ ), where  $\lambda_{\text{peak}}$  is the wavelength of the first order diffracted light at the maximum intensity,  $n$  is the average effective index of refraction,  $d$  is the lattice spacing between the two consecutive layers, and  $\theta$  is the angle of incidence of the incoming illumination. We fabricated a  $\sim 10 \mu\text{m}$  thick hydrogel, which can theoretically accommodate 54 fringes. In order to cause a resolvable spectral shift, the hydrogel needs to swell a minimum of  $\sim 9.7 \text{ nm}$ .

We have developed a viable platform technology to fabricate tunable holographic sensors via laser light. We have reported

the use of a laser pulse (6 ns, 240 mJ) to organize an on-axis 3D tunable sensor consisting of well-ordered silver nanoparticles embedded within a hydrogel matrix. The holographic sensor can be finely modulated to diffract narrow-band light based on changes in nanoparticle spacing and index of refraction. Our work demonstrates that holographic sensors display large reversible band gap tunability in response to variations in pH. These holographic sensors diffract light from the visible region to the near-infrared region ( $\lambda_{\text{peak}} \approx 495\text{--}815 \text{ nm}$ ). The clinical application of our holographic sensors was demonstrated by pH sensing of artificial urine over the physiological range (4.5–9.0), with exceptional sensitivity between pH 5.0 and 6.0.

Our method allows the use of a diverse array of substrate matrices, ranging from synthetic to natural polymers. The diffraction angle and holographic pattern within the matrix can also be controlled depending on the desired application. Other metallic nanoparticles and dyes can also be used in building well-ordered diffraction gratings with our method. Our sensing platform has extremely attractive attributes such as simple fabrication without requiring cleanroom facilities, flexible characteristics desirable for printing, and overall low-cost with potential scalability. We anticipate that our platform strategy of fabricating label-free holographic sensors with wide optical ranges will lead to many novel applications from printable diffraction grating devices to rapid colorimetric sensors and biomedical sensing.

## Experimental Section

**Materials and Instruments:** 2-Hydroxyethyl methacrylate (HEMA) (ultrapure 99+%), ethylene glycol dimethacrylate (EDMA) (98%), methacrylic acid (MAA) (99%), 2,2-dimethoxy-2-phenylacetophenone (DMPA) (99%), silver nitrate (99%), citric acid (99.5%), sodium phosphate dibasic ( $\text{Na}_2\text{HPO}_4$ ) (99.0%), L-ascorbic acid (99%), sodium carbonate (99.9%) and sodium hydroxide (98.0%) were purchased from Sigma-Aldrich, UK. 4-methylaminophenol sulfate (99%) was purchased from Acros Organics, UK. Poly(methyl methacrylate) (PMMA) (0.5 mm thick) was purchased from Goodfellow Cambridge Ltd (Huntingdon, UK). Citric acid –  $\text{Na}_2\text{HPO}_4$  buffer solutions (150 mM) were used to obtain desired pH values.

Femto plasma cleaner (Diener electronic, Ebhausen, Germany) was used under 1 torr vacuum. Single-side aluminized polyester film was purchased from HiFi Industrial Film Ltd. (Stevenage, UK). Stratalinker 2400 UV Crosslinker ( $\sim 350 \text{ nm}$ ,  $4000 \mu\text{watts}/\text{cm}^2$ ) was purchased from RS Components (Corby, UK). Nd-Yttrium-Aluminum-Garnet pulsed laser (high power compact Qswitched Nd:YAG oscillator with super gaussian resonator, 700 mJ @ 1064 nm, 10 Hz) with a second harmonic generator, 350 mJ @ 532 nm 10 Hz, thermally stabilized with wavelength separation) and supercontinuum white light laser were purchased from Lambda Photometrics (Harpending, UK) and Fianium (SC400, Eugene, OR), respectively. AvaSpec 2028 spectrophotometer, 2048-pixel InstaSpec IV CCD detector, QE6500 spectrometer and a bifurcated cable (FC UV 600-2, 600  $\mu\text{m}$  fiber, 2 m length, SMA terminations) were purchased from Avantes (Apeldoorn, The Netherlands) and Ocean Optics (Dunedin, FL). FE20 FiveEasy pH meter was purchased from Mettler Toledo (Leicester, UK). Abbé refractometer (Atago 4t) with an LED was purchased from Atago USA (Bellevue, WA). A plano-convex lens (laser grade PCX lens, 25 mm diameter x 75 mm FL, uncoated) was purchased from Edmund Optics Ltd. (York, UK). AvaSoft (v7.5) software, Igor Pro, MATLAB (v8.1) and COMSOL Multiphysics (v4.3b) were used for data processing and simulations. Lumix DMC-FZ20 camera was used for imaging. TEM images were obtained on a FEI Tecnai G2 (Oregon, USA) operated at 120 kV. Images were recorded with an AMT 60B camera running Deben software.

**Preparation of Holographic Sensors:** HEMA (91.5 mol%), EDMA (2.5 mol%), MAA (6 mol%) solution was mixed with equal volume of 2% (w:v) DMPA in isopropanol, cast and polymerized onto PMMA substrates previously treated with O<sub>2</sub> plasma. The hydrogel thickness was controlled to be approximately 10 μm. Ag<sup>0</sup> nanoparticles (~10–100 nm in diameter) were prepared through the incorporation and reduction of aqueous AgNO<sub>3</sub> (1 M) within the hydrogel. Well-ordered Ag<sup>0</sup> nanoparticle structures within the hydrogel were formed via a single 6-ns pulse of laser beam directed at the sample elevated at 5° from the normal, backed by a mirror and immersed in aqueous solution at pH 4.0 (see Supporting Information).

## Supporting Information

Supporting Information is available from the Wiley Online Library or from the author.

## Acknowledgements

We thank Michael Monteiro and Caterina Ducati for useful discussions. F.C.V. would like to thank the Postdoctoral Fellowships from FAPESP (Grant No. 2011/06906-6) and CNPq INCTBio (Grant No. 209869/2013-5).

Received: September 7, 2013

Revised: December 5, 2013

Published online:

- [1] a) Y. Kang, J. J. Walsh, T. Gorishnyy, E. L. Thomas, *Nat. Mater.* **2007**, *6*, 957–960; b) H. Kim, J. Ge, J. Kim, S.-e. Choi, H. Lee, H. Lee, W. Park, Y. Yin, S. Kwon, *Nat. Photon.* **2009**, *3*, 534–540; c) S. Kim, A. N. Mitropoulos, J. D. Spitzberg, H. Tao, D. L. Kaplan, F. G. Omenetto, *Nat. Photon.* **2012**, *6*, 818–823.
- [2] a) Y. Y. Li, F. Cunin, J. R. Link, T. Gao, R. E. Betts, S. H. Reiver, V. Chin, S. N. Bhatia, M. J. Sailor, *Science* **2003**, *299*, 2045–2047; b) J. Kim, J. Yoon, R. C. Hayward, *Nat. Mater.* **2010**, *9*, 159–164.
- [3] a) S. O. Kim, H. H. Solak, M. P. Stoykovich, N. J. Ferrier, J. J. De Pablo, P. F. Nealey, *Nature* **2003**, *424*, 411–414; b) S. Ogawa, M. Imada, S. Yoshimoto, M. Okano, S. Noda, *Science* **2004**, *305*, 227–229; c) M. Deubel, G. von Freymann, M. Wegener, S. Pereira, K. Busch, C. M. Soukoulis, *Nat. Mater.* **2004**, *3*, 444–447; d) M. Qi, E. Lidorikis, P. T. Rakich, S. G. Johnson, J. D. Joannopoulos, E. P. Ippen, H. I. Smith, *Nature* **2004**, *429*, 538–542; e) A. C. Arsenault, T. J. Clark, G. von Freymann, L. Cademartiri, R. Sapienza, J. Bertolotti, E. Vekris, S. Wong, V. Kitaev, I. Manners, R. Z. Wang, S. John, D. Wiersma, G. a. Ozin, *Nat. Mater.* **2006**, *5*, 179–184; f) K. Aoki, D. Guimard, M. Nishioka, M. Nomura, S. Iwamoto, Y. Arakawa, *Nat. Photon.* **2008**, *2*, 688–692; g) J. S. Skibina, R. Iliw, J. Bethge, M. Bock, D. Fischer, V. I. Beloglasov, R. Wedell, G. Steinmeyer, *Nat. Photon.* **2008**, *2*, 679–683; h) S. A. Rinne, F. Garcia-Santamaria, P. V. Braun, *Nat. Photon.* **2008**, *2*, 52–56; i) S. Takahashi, K. Suzuki, M. Okano, M. Imada, T. Nakamori, Y. Ota, K. Ishizaki, S. Noda, *Nat. Mater.* **2009**, *8*, 721–725; j) K. Ishizaki, S. Noda, *Nature* **2009**, *460*, 367–370; k) Y. Fuchs, O. Soppera, A. G. Mayes, K. Haupt, *Adv. Mater.* **2013**, *25*, 566–570; l) A. Llordes, G. Garcia, J. Gazquez, D. J. Milliron, *Nature* **2013**, *500*, 323–326; m) M. Kolle, A. Lethbridge, M. Kreysing, J. J. Baumberg, J. Aizenberg, P. Vukusic, *Adv. Mater.* **2013**, *25*, 2239–2245.
- [4] a) C. A. B. Davidson, J. Blyth, C. R. Lowe, *WO 2010041079 A1* **2010**; b) J. L. Martinez-Hurtado, C. A. Davidson, J. Blyth, C. R. Lowe, *Langmuir* **2010**, *26*, 15694–15699; c) J. L. Martinez-Hurtado, C. A. B. Davidson, C. R. Lowe, *Proc. SPIE* **2011**, *8024*.
- [5] S. A. Benton, V. M. Bove, In-Line “Denisyuk” Reflection Holography, John Wiley & Sons, Inc., USA **2007**.
- [6] a) Y. Fuchs, S. Kunath, O. Soppera, K. Haupt, A. G. Mayes, *Adv. Funct. Mater.* **2013**, n/a–n/a; b) A. G. Mayes, J. Blyth, R. B. Millington, C. R. Lowe, *J. Mol. Recognit.* **1998**, *11*, 168–174; c) V. Toal, Introduction to Holography, Chapter 17: Holographic Sensors and Indicators, CRC Press, USA **2012**; d) A. J. Marshall, J. Blyth, C. a. B. Davidson, C. R. Lowe, *Analyt. Chem.* **2003**, *75*, 4423–4431.
- [7] M. A. Makos, D. M. Omiattek, A. G. Ewing, M. L. Heien, *Langmuir* **2010**, *26*, 10386–10391.
- [8] B. R. Huang, T. C. Lin, *Appl. Phys. Lett.* **2011**, *99*, 023108.
- [9] S. Modi, M. G. Swetha, D. Goswami, G. D. Gupta, S. Mayor, Y. Krishnan, *Nat. Nanotechnol.* **2009**, *4*, 325–330.
- [10] M. Tantama, Y. P. Hung, G. Yellen, *J. Am. Chem. Soc.* **2011**, *133*, 10034–10037.
- [11] A. Grover, B. F. Schmidt, R. D. Salter, S. C. Watkins, A. S. Waggoner, M. P. Bruchez, *Angew. Chem. Int. Ed.* **2012**, *51*, 4838–4842.
- [12] a) J. D. Ehrick, S. K. Deo, T. W. Browning, L. G. Bachas, M. J. Madou, S. Daunert, *Nat. Mater.* **2005**, *4*, 298–302; b) A. Lendlein, H. Jiang, O. Junger, R. Langer, *Nature* **2005**, *434*, 879–882; c) S. H. Um, J. B. Lee, N. Park, S. Y. Kwon, C. C. Umbach, D. Luo, *Nat. Mater.* **2006**, *5*, 797–801; d) M. Ehrbar, R. Schoenmakers, E. H. Christen, M. Fussenegger, W. Weber, *Nat. Mater.* **2008**, *7*, 800–804; e) A. M. Kloxin, A. M. Kasko, C. N. Salinas, K. S. Anseth, *Science* **2009**, *324*, 59–63; f) E. F. Banwell, E. S. Abelardo, D. J. Adams, M. a. Birchall, A. Corrigan, A. M. Donald, M. Kirkland, L. C. Serpell, M. F. Butler, D. N. Woolfson, *Nat. Mater.* **2009**, *8*, 596–600; g) M. A. C. Stuart, W. T. S. Huck, J. Genzer, M. Muller, C. Ober, M. Stamm, G. B. Sukhorukov, I. Szleifer, V. V. Tsukruk, M. Urban, F. Winnik, S. Zauscher, I. Luzinov, S. Minko, *Nat. Mater.* **2010**, *9*, 101–113.
- [13] a) V. Toal, Introduction to Holography, Chapter 1: Light, Waves, and Rays, CRC Press, USA **2012**; b) J. D. Joannopoulos, S. G. Johnson, J. N. Winn, R. D. Meade, Photonic Crystals: Molding the Flow of Light, Chapter 3: Symmetries and Solid-State Electromagnetism, 2nd ed., Princeton University Press, New Jersey **2008**; c) T. V. Teperik, V. V. Popov, F. J. Garcia de Abajo, M. Abdelsalam, P. N. Bartlett, T. A. Kelf, Y. Sugawara, J. J. Baumberg, *Opt. Express* **2006**, *14*, 1965–1972.
- [14] a) M. Dell’Aglio, R. Gaudio, R. ElRashedy, O. De Pascale, G. Palazzo, A. De Giacomo, *Phys. Chem. Chem. Phys.* **2013**, *15*, 20868–20875; b) P. Wagener, S. Ibrahimkuty, A. Menzel, A. Plech, S. Barcikowski, *Phys. Chem. Chem. Phys.* **2013**, *15*, 3068–3074; c) B. Toftmann, B. Doggett, C. B. J. Rgensen, J. Schou, J. G. Lunney, *J. Appl. Phys.* **2013**, *113*.
- [15] a) J. Chung, S. Han, D. Lee, S. Ahn, C. P. Grigoropoulos, J. Moon, S. H. Ko, *Opt. Engineering* **2013**, *52*, 024302; b) V. N. Bagratashvili, A. O. Rybaltovskiy, N. V. Minaev, P. S. Timashev, V. V. Firsov, V. I. Yusupov, *Laser Phys. Lett.* **2010**, *7*, 401–404; c) A. O. Rybaltovskii, V. I. Gerasimova, N. V. Minaev, V. I. Sokolov, P. S. Timashev, E. A. Troitskaya, V. V. Firsov, V. I. Yusupov, V. N. Bagratashvili, *Nanotechnol. Russia* **2010**, *5*, 435–445.
- [16] A. W. Martinez, S. T. Phillips, G. M. Whitesides, *Proc. Natl. Acad. Sci. USA* **2008**, *105*, 19606–19611.
- [17] A. Kratz, M. Ferraro, P. M. Sluss, K. B. Lewandrowski, *New Engl. J. Med.* **2004**, *351*, 1548–1563.
- [18] J. A. Simerville, W. C. Maxted, J. J. Pahira, *Am. Family Physician* **2005**, *71*, 1153–1162.
- [19] J. Rodríguez Soriano, *J. Am. Soc. Nephrology* **2002**, *13*, 2160–2170.
- [20] a) H. Hesse, D. Heimbach, *World J. Urology* **1999**, *17*, 308–315; b) B. H. Eisner, D. S. Goldfarb, G. Pareek, *Urologic Clinics North Am.* **2013**, *40*, 21–30.
- [21] A. T. Proudfoot, E. P. Krenzelo, J. A. Vale, *J. Toxicol. Clin. Toxicol.* **2004**, *42*, 1–26.